

Tensor networks for unsupervised machine learning

Jing Liu,¹ Sujie Li,^{2,3} Jiang Zhang,¹ and Pan Zhang^{2,4,5,*}

¹*School of Systems Science, Beijing Normal University*

²*CAS Key Laboratory for Theoretical Physics, Institute of Theoretical Physics,*

Chinese Academy of Sciences, Beijing 100190, China

³*School of Physical Sciences, University of Chinese Academy of Sciences, Beijing 100049, China*

⁴*School of Fundamental Physics and Mathematical Sciences,*

Hangzhou Institute for Advanced Study, UCAS, Hangzhou 310024, China

⁵*International Centre for Theoretical Physics Asia-Pacific, Beijing/Hangzhou, China*

(Dated: June 25, 2021)

Modeling the joint distribution of high-dimensional data is a central task in unsupervised machine learning. In recent years, many interests have been attracted to developing learning models based on tensor networks, which have advantages of theoretical understandings of the expressive power using entanglement properties, and as a bridge connecting the classical computation and the quantum computation. Despite the great potential, however, existing tensor-network-based unsupervised models only work as a proof of principle, as their performances are much worse than the standard models such as the restricted Boltzmann machines and neural networks. In this work, we present the Autoregressive Matrix Product States (AMPS), a tensor-network-based model combining the matrix product states from quantum many-body physics and the autoregressive models from machine learning. The model enjoys exact calculation of normalized probability and unbiased sampling, as well as a clear theoretical understanding of expressive power. We demonstrate the performance of our model using two applications, the generative modeling on synthetic and real-world data, and the reinforcement learning in statistical physics. Using extensive numerical experiments, we show that the proposed model significantly outperforms the existing tensor-network-based models and the restricted Boltzmann machines, and is competitive with the state-of-the-art neural network models.

Unsupervised learning aims to understand the high dimensional data \mathbf{x} with rich structures, by learning a probability distribution $P(\mathbf{x})$ from the data. The central challenge is how to represent the joint distribution with an exponential number of entries using a polynomial number of parameters and how to efficiently sample from it. Indeed, even computing the normalization constant for a general joint distribution belongs to the #P hard problem, and has attracted enormous efforts [1, 2] in the past decades. From the point of view of computations, unsupervised learning shares the same challenges with statistical physics and quantum many-body physics, where the target distribution or the target quantum state one investigates lives in a huge space and is difficult to control. In the history of machine learning, many classical models were inspired by physics.

One of the most important unsupervised model, the celebrated *Boltzmann machine* [3, 4], was inspired by statistical physics, where $P(\mathbf{x})$ is expressed using the Boltzmann distribution with parameters encoded in the energy function $E(\mathbf{x})$,

$$P(\mathbf{x}) = \frac{1}{Z} e^{-\beta E(\mathbf{x})}. \quad (1)$$

To efficiently sample from the Boltzmann distribution, the model is usually defined on a bipartite graph where efficient block-update Monte Carlo methods exist. This is known as the *restricted Boltzmann machine* (RBM) [5, 6] and has found numerous applications in machine learning and physics. Another physics-inspired model is the *Born machine* [7, 8], where the joint distribution of variable is modeled by squared norm of a quantum state Ψ , with

$$P(\mathbf{x}) = \frac{1}{Z} |\Psi(x_1, x_2, \dots, x_n)|^2, \quad (2)$$

with the wave function represented by a tensor network [7–10]. Given the probabilistic interpretations of quantum mechanics, as well as the close relations between tensor networks and quantum circuits, the Born machines have potential applications in quantum machine learning.

Theoretically, tensor network models based on matrix product states (MPS) [7, 11] and tree tensor networks (TTN) [9, 12] enjoy tractable normalization and a good theoretical interpretation of the representation power. However, it is somehow embarrassing that when applied to practical unsupervised learning tasks on the standard dataset, the performance of tensor-network-based models is much worse [7, 9] than the neural-network-based models, even has a significant gap to the RBM which was invented more than 30 years ago [3, 4].

In this work, we aim to fill this gap. Based on the matrix product states, we propose an unsupervised model which maintains the advantages with tractable normalization and exact sampling, while has much stronger representation power than the matrix product states Born machine [7]. In the proposed model, instead of representing a joint distribution $P(\mathbf{x})$ directly using a tensor network, we combine it to the autoregressive construction of joint probabilities, by factorizing the joint probability as a product of conditional probabilities. We coin our model as *Autoregressive Matrix Product States* (AMPS). For the theoretical representation power, the model has a two-dimensional tensor network representation, which has similar entanglement structures with the two-dimensional tensor network representation of the RBM [13], while has the ability of computing the exact normalized probability and unbiased directly sampling. For applications, by varying parameters of the conditional probabilities, i.e. tensor elements of MPSs, we can

train the model to accomplish various machine learning tasks. In the generative learning (or density estimation) tasks [2], we learn the data distribution using $P(\mathbf{x})$ by minimizing the forward KL divergence between data distribution and AMPS $D_{\text{KL}}(P_{\text{data}}\|P(\mathbf{x}))$; in the reinforcement learning of statistical physics [14] we learn the Boltzmann distribution using $P(\mathbf{x})$ by minimizing the reverse KL divergence between the AMPS and the Boltzmann distribution $D_{\text{KL}}(P(\mathbf{x})\|P_{\text{Boltzmann}})$ with the REINFORCE [15] algorithm. Using numerical experiments, we show that in these two applications, the performance of AMPS is much stronger than existing tensor-network-based models and is competitive to the neural network models.

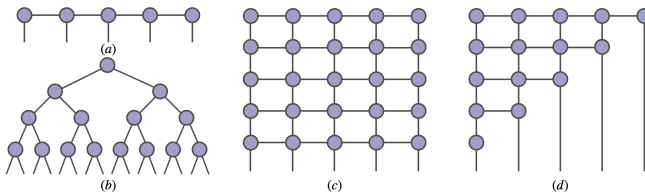


Figure 1. Schematic representation of generative models based on (a) Matrix Product States, (b) Tree Tensor Networks, (c) restricted Boltzmann machine (with the two-dimensional representation proposed in [13]), and (d) Autoregressive Matrix Product States.

Autoregressive Matrix Product States— The standard tensor networks in quantum many-body physics, such as the matrix product states and tree tensor networks (as illustrated in Fig. 1), have been generalized to unsupervised modeling [7, 9, 10]. The obtained generative models have advantages of exact computation of normalized probabilities and directly sampling. However, when applied to generative learning tasks on the standard datasets, their performances have a significant gap [7, 9] to the restricted Boltzmann machines and neural networks. The starting point of this work is to understand the reason behind the gap and to investigate how to fill it.

Interestingly, as reported in [13], RBM itself can be interpreted as a tensor network model in two dimension [13]. In detail, an RBM with n visible neurons and m hidden neurons can be interpreted as a two-dimensional tensor network with m rows and n columns, with each row representing an MPS (see Fig. 1(c)), we refer to appendices and [13] for more details. In other words, an RBM can be regarded as a product of MPSs [10, 16]. From the figure, we observe that if we squeeze all m layers from top to bottom, we essentially arrive at an MPS (see Fig. 1(a)) with bond dimension 2^m . This indicates that the RBM can be understood as a further factorization of a MPS, hence exhibits a much higher parameter efficiency: an RBM with m hidden variables could represent a probability tensor with CP rank at most 2^m , using mn parameters, while a vanilla MPS model requires about $n2^{2m}$ parameters [7]. Thus, the advantage in the expressive power of RBM with respect to the MPS essentially comes from the product rule. However, the defects associated with the product of MPSs in RBM are that as opposed to a single MPS, the normalization of the joint probability associated with the two-dimensional tensor

network is not tractable, and the resulted distribution can not be directly sampled.

Then a natural question arises is can we keep the representation power with the product of MPSs, while preserving tractability of sampling and normalization computation? In this work, we answer this question by proposing the autoregressive matrix product states (AMPS). As illustrated in Fig. 1, the proposed tensor network is also designed as a product of factors, with each factor $\Psi_{x_1 x_2 \dots x_i}^{(i)}$ has a different length, with

$$P(\mathbf{x}) = \frac{1}{\tilde{Z}} \Psi_{x_1}^{(1)} \Psi_{x_1 x_2}^{(2)} \dots \Psi_{x_1 x_2 \dots x_n}^{(n)}. \quad (3)$$

The difference between Ψ and the MPS in the two-dimensional tensor network representation of RBM is that it is designed to normalize such that $\sum_{x_i} \Psi_{(x_1 x_2 \dots x_i)}^{(i)} = 1$, meaning that $\Psi_{(x_1 x_2 \dots x_i)}^{(i)}$ expresses conditional probability $P(x_i | x_1, \dots, x_{i-1})$. This is also known as autoregressive modeling in machine learning.

We propose to represent each factor using a matrix product state [11, 17]

$$\psi_{x_1 x_2 \dots x_n} = \sum_{\alpha_0, \alpha_1, \dots, \alpha_n} A_{x_1 \alpha_0 \alpha_1}^{(1)} A_{x_2 \alpha_1 \alpha_2}^{(2)} \dots A_{x_{n-1} \alpha_{n-1} \alpha_n}^{(n)},$$

where $A^{(i)} \in \mathbb{R}^{2 \times D_{i-1} \times D_i}$ is a three-way tensor. The first index x_i corresponds to the physical variable x_i , the second index α_{i-1} corresponds to the interaction to the previous tensor $A^{(i-1)}$, with (bond) dimension D_{i-1} , and the last index α_i corresponds to the interaction to the next tensor $A^{(i+1)}$, with (bond) dimension D_i . In order to express a conditional distribution, Ψ must be non-negative. There are several ways to ensure this condition. One way is (as in the Born machines [7]) to normalize using the squared norm of ψ : $\Psi_{x_1 x_2 \dots x_n}^{(n)} = \frac{1}{\tilde{Z}} |\psi_{x_1 x_2 \dots x_n}|^2$, where \tilde{Z} is the normalizing factor. Another way is to use exponential parameterization of ψ , as $\Psi_{x_1 x_2 \dots x_n}^{(n)} = \frac{e^{\psi_{x_1 x_2 \dots x_n}}}{\sum_{x_n} e^{\psi_{x_1 x_2 \dots x_n}}}$. Moreover, one can impose non-negative condition for every tensor element in ψ . We found that the second choice, the exponential function works best in practice.

AMPS for generative modeling— Generative modeling asks to learn parameters of $P(\mathbf{x})$ in form of Eq. (3) as close as possible to the empirical distribution of given data set \mathcal{T} [2, 18], by minimizing the negative log-likelihood (NLL) \mathcal{L} , which is equivalent to minimizing the KL divergence between the empirical data distribution and $P(\mathbf{x})$. In this work, we assume that the data variables are binary, i.e. $\mathbf{x} \in \{0, 1\}^n$ for each data sample containing n variables. After the minimization, the achieved \mathcal{L} of the model quantifies the performance of the learned model in representing the training dataset. The lower bound for \mathcal{L} is the entropy of the empirical data distribution, which equals to $\ln |\mathcal{T}|$ if there are no duplications.

First, we study the case when the training data are random samples. How many random patterns can be remembered by the model indicates the expressive power of the model, also known as model capacity [19]. When $|\mathcal{T}|$ random patterns are

exactly remembered, the negative log-likelihood of the model would be $\log(|\mathcal{T}|)$, and the learned distribution faithfully represents the empirical distribution with $|\mathcal{T}|$ nonzero values.

In the experimental evaluations, we plot \mathcal{L} obtained in AMPS as a function of the number of patterns $|\mathcal{T}|$, and compared to MPS Born machines [7] with the different bond dimensions and RBMs with different number of hidden variables, trained on the same data. We chose a small number of variables $n = 20$ so that the partition function of RBM, the gradients of parameters, as well as its log-likelihood, can be computed exactly. The results are reported in Fig. 2 where the lower bound for \mathcal{L} are shown as the dashed line. We see that with more hidden variables, RBM has more parameters ($n \times h$) and is more expressive, giving a smaller \mathcal{L} . Similarly with a larger bond dimension D , The MPS Born machine also contains more parameters (ND^2) and obtains a smaller \mathcal{L} . In particular, with $D \geq |\mathcal{T}|$, the MPS Born machine is able to faithfully clone the empirical data distribution [7] and gives $\mathcal{L} = \ln |\mathcal{T}|$. The figure demonstrates that with a small bond dimension $D = 10$, the proposed AMPS already significantly outperforms RBM with $h = 300$ hidden variables, and Born Machine with $D = 160$, exhibiting a much stronger expressive power than both RBM and MPS. We have also investigated unsupervised learning on real-world datasets studied in [10] and evaluated its performance with other tensor network models such as the MPS Born machine with complex entries and the Locally Purified States (LPS) [10]. The results are shown in Fig. 2b, where we can see that with the same bond dimension, AMPS is significantly superior to other tensor network models, obtaining much lower NLL with fewer parameters. In particular, with a bond dimension larger than 3, AMPS achieves \mathcal{L} equals to the lower bound, which is already beyond the reach of other tensor-network models with a large number of parameters. More evaluations on the random datasets and a variety of real-world datasets can be found in the appendices, where the results further confirm the superiority of AMPS in both performance and the parameter efficiency.

Next, to demonstrate the generalization ability, we perform experiments on the binarized MNIST [21, 22] dataset, a standard benchmark for generative models in machine learning. The binary MNIST dataset contains 50,000 training images of handwritten digits, 10,000 validation and 10,000 test images. Each image is composed of 28×28 binary pixels. We force all MPSs in the AMPS to totally share the parameters, this greatly improves the generalization power and reduces the number of parameters. We use the overall 50,000 images in the training set to learn an AMPS with sharing parameters and report the averaged NLL on the 10,000 images in the test dataset. The results are summarized in Table I, benchmarked with the MPS Born machine [7], the Tree Tensor Network Born machine [9], and the generative models using deep neural networks: NADE [23], MADE [24], and PixelCNN [25]. Among them, PixelCNN uses convolutional neural networks while NADE and MADE are non-convolution neural networks. The test NLL given by AMPS is 84.1, with a corresponding bond dimension $D = 100$, which greatly improves over the

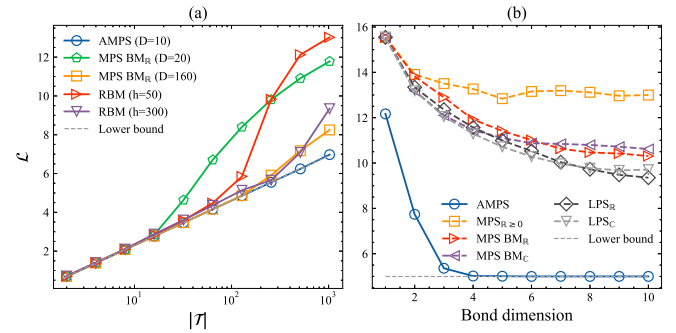


Figure 2. (a) For random datasets with $n = 20$ variables, we plot the negative log-likelihood \mathcal{L} as a function of the number of samples $|\mathcal{T}|$ for AMPS, matrix product states Born machine with real entries (MPS BM_R) with various bond dimensions D , and the restricted Boltzmann machine (RBM) with various number of hidden neurons h . (b) For the real-world dataset Lymphography [20], we plot the negative log-likelihood \mathcal{L} as a function of bond dimension D for AMPS, matrix product states Born machine with real entries (MPS BM_R), complex entries (MPS BM_C), non-negative entries (MPS $_{\mathbb{R} \geq 0}$) respectively, and locally purified states with real entries (LPS R) and complex entries (LPS C). Lower bounds of \mathcal{L} are determined using the entropy of the empirical data distribution.

existing tensor-network-based models. Remarkably, AMPS is competitive with state-of-the-art deep generative models, even outperforms non-convolutional neural networks MADE and NADE. We also see from the figure that there is an NLL gap between AMPS and the PixelCNN (which is considered as one of the state-of-the-art models for density estimation). The reason for the gap is clearly the absence of the convolutional structure in AMPS on the image data. Therefore, we incorporate the convolutional structure into AMPS, which is termed as *Convolution-AMPS*, and evaluate its performance on the binary MNIST dataset in Table I. We can see that the obtained NLL is very close to the PixelCNN. The details of incorporating convolutions and AMPS can be found in appendices.

Thanks to modeling every conditional probability in AMPS, we are able to sample pixels one by one from the learned distribution in an unbiased way, which is known as *Ascension Sampling* [1] in machine learning. To visually illustrate the quality of images generated by the learned AMPS and Convolution-AMPS, in Fig. 3(b) and Fig. 3(c) we randomly sample 36 images from AMPS with bond dimension $D = 100$ and Convolution-AMPS with 8 layers and $D = 14$ respectively, trained on the binary MNIST dataset. We can see that most of the digit numbers in Fig. 3(b) and Fig. 3(c) are recognizable and is visually very close to the original handwritten digits in Fig. 3(a).

AMPS for reinforcement learning in statistical physics.— Reinforcement learning [27] has many applications in artificial intelligence [28], as well as in physics, e.g. as a variational method in statistical mechanics [14, 29] and in quantum many-body physics [30, 31]. For the statistical mechanics problems, reinforcement learning is used to minimize the variational free energy F_q of a variational distribution $q_\theta(\mathbf{x})$, an upper bound

Non-convolution Models		Test NLL
MPS Born Machine		101.5 [7, 9]
TTN-1d		96.9 [9]
TTN-2d		94.3 [9]
RBM		86.3* [26]
NADE		88.3 [23]
MADE		86.6 [24]
AMPS		84.1

Convolution Models		Test NLL
PixelCNN		81.3 [25]
Convolution-AMPS		81.8

Table I. Negative log-likelihood on test dataset (Test NLL, the smaller the better) given by AMPS on the binarized MNIST dataset, compared with various tensor network models and neural network models. For RBM, the * stands for an approximated NLL, because the exact NLL is not computable for RBM on the MNIST dataset.

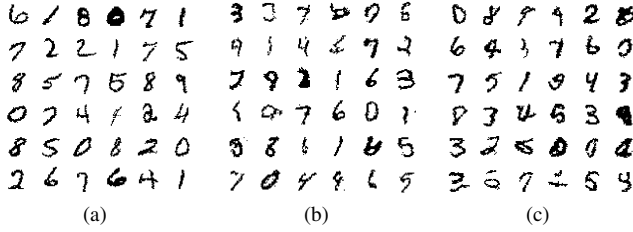


Figure 3. (a) Handwritten digit images sampled from the binarized MNIST dataset; (b) Images sampled from the learned AMPS with parameter sharing with $D = 100$, test NLL = 84.1; (c) Images sampled from the learned Convolution-AMPS with eight layers and the bond dimension $D = 14$, test NLL = 81.8.

of the true free energy of the Boltzmann distribution:

$$F_q = \frac{1}{\beta} \sum_x q_\theta(x) [\beta E(x) + \ln q_\theta(x)]. \quad (4)$$

In the standard mean-field methods such as the variational mean-field method and the Bethe approximation, $q_\theta(x)$ is chosen in a simple form such that the variational free energy and its derivatives with respect to the parameters of $q_\theta(x)$ can be expressed analytically. In the recently proposed variational autoregressive networks (VAN) [14, 29], the $q_\theta(x)$ is parameterized using deep neural networks, which achieves the state-of-the-art results in obtaining variational free energies in spin glasses. In this work, we show that AMPS can be applied as a variational distribution $q_{\text{AMPS}}(x)$ for minimizing the free energy F_q (4) reinforcement learning, achieving competitive performance to the neural network models.

To evaluate the performance of the AMPS-based reinforcement learning, we perform experiments on the celebrated Sherrington-Kirkpatrick (SK) spin-glass model [33]. The energy of a configuration x is defined as $E(x) = -\sum_{1 \leq i < j \leq n} J_{ij} s_i s_j$ where the couplings $J_{ij} = J_{ji}$ follow Gaussian distribution with 0 mean and variance $1/\sqrt{n}$, with n denoting the number of spins. We follow the experimental settings

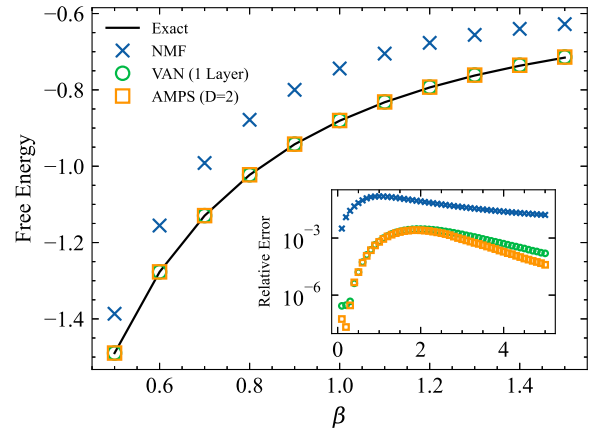


Figure 4. Free energy obtained by the Naïve mean-field [32] (NMF), variational autoregressive network (VAN) [14] and the AMPS on the Sherrington-Kirkpatrick spin-glass model [33] with $n = 20$ spins. The inset plot shows the relative error on a logarithmic scale. In the experiments, the VAN and AMPS have roughly the same amount of parameters.

in VAN [14] and choose the system size $n = 20$ in order to enumerate all 2^n configurations for computing the exact free energy for the evaluations. The obtained free energies are shown in Fig. (4) and compared against VAN and mean-field methods. We can see that AMPS with $D = 2$ achieves competitive results with VAN which has the same number of parameters, both significantly outperform the classic mean-field methods such as the naïve mean field (NMF). Remarkably, at both high temperatures (small β) and low temperatures (large β), the AMPS gives better results than the VAN.

Discussions— We have presented the AMPS, a tensor-network-based model for unsupervised machine learning. The model incorporates autoregressive modeling in machine learning and the matrix product states in physics. It enjoys the exact computation of joint probability which is inherited from the autoregressive model, as well as the theoretical understanding of expressive power from the viewpoint of entanglement structures which is inherited from the matrix product states. Theoretically, the expressive power of the AMPS is much stronger than existing tensor-network generative models. Empirically, using extensive experiments we demonstrated that the AMPS outperforms existing tensor network models in generative modeling of images, and reinforcement learning in variational statistical mechanics of spin glasses. Remarkably, its performance is competitive with the state-of-the-art deep neural network models, even better in some cases. This uncovers the great potential of tensor networks in machine learning. Finally, we note that with natural relations between tensor networks and quantum circuits [34–36], it would be interesting to further investigate along this line for combining autoregressive modeling and quantum machine learning.

P.Z. is supported by CAS Grant No. QYZDB-SSW-SYS032, and Project 11747601 and 11975294 of NSFC. We provide Pytorch implementations of the algorithm at [37].

* panzhang@itp.ac.cn

[1] C. M. Bishop, *Pattern recognition and machine learning* (springer, 2006).

[2] I. Goodfellow, Y. Bengio, and A. Courville, *Deep Learning* (The MIT Press, 2016).

[3] G. E. Hinton and T. J. Sejnowski, Optimal perceptual inference, in *Proceedings of the IEEE conference on Computer Vision and Pattern Recognition*, Vol. 448 (Citeseer, 1983).

[4] P. Smolensky, *Information processing in dynamical systems: Foundations of harmony theory*, Tech. Rep. (Colorado Univ at Boulder Dept of Computer Science, 1986).

[5] G. E. Hinton, Training products of experts by minimizing contrastive divergence, *Neural computation* **14**, 1771 (2002).

[6] G. E. Hinton and R. R. Salakhutdinov, Reducing the dimensionality of data with neural networks, *Science* **313**, 504 (2006).

[7] Z.-Y. Han, J. Wang, H. Fan, L. Wang, and P. Zhang, Unsupervised generative modeling using matrix product states, *Physical Review X* **8**, 031012 (2018).

[8] S. Cheng, J. Chen, and L. Wang, Information perspective to probabilistic modeling: Boltzmann machines versus born machines, *Entropy* **20**, 583 (2018).

[9] S. Cheng, L. Wang, T. Xiang, and P. Zhang, Tree tensor networks for generative modeling, *Physical Review B* **99**, 155131 (2019).

[10] I. Glasser, R. Sweke, N. Pancotti, J. Eisert, and I. Cirac, Expressive power of tensor-network factorizations for probabilistic modeling, in *Advances in Neural Information Processing Systems* (2019) pp. 1498–1510.

[11] D. Pérez-García, F. Verstraete, M. Wolf, and J. Cirac, Matrix product state representations, *Quantum Inf. Comput.* **7**, 401 (2007).

[12] Y. Y. Shi, L. M. Duan, and G. Vidal, Classical simulation of quantum many-body systems with a tree tensor network, *Physical Review A* **74**, 154 (2006).

[13] S. Li, F. Pan, P. Zhou, and P. Zhang, Boltzmann machines as two-dimensional tensor networks, *arXiv preprint arXiv:2105.04130* (2021).

[14] D. Wu, L. Wang, and P. Zhang, Solving statistical mechanics using variational autoregressive networks, *Physical Review Letters* **122**, 080602 (2019).

[15] R. J. Williams, Simple statistical gradient-following algorithms for connectionist reinforcement learning, *Machine learning* **8**, 229 (1992).

[16] S. R. Clark, Unifying neural-network quantum states and correlator product states via tensor networks, *Journal of Physics A: Mathematical and Theoretical* **51**, 135301 (2018).

[17] U. Schollwöck, The density-matrix renormalization group in the age of matrix product states, *Annals of physics* **326**, 96 (2011).

[18] Y. LeCun, Y. Bengio, and G. Hinton, Deep learning, *Nature* **521**, 436 (2015).

[19] J. J. Hopfield, Neural networks and physical systems with emergent collective computational abilities, *Proceedings of the national academy of sciences* **79**, 2554 (1982).

[20] The lymphography domain obtained from the university medical centre, institute of oncology, ljubljana, yugoslavia.

[21] Y. LeCun, C. Cortes, and C. J. Burges, The mnist database of handwritten digits (1998), <http://yann.lecun.com/exdb/mnist>.

[22] http://www.dmi.usherb.ca/~larocheh/mlpython/_modules/datasets/binarized_mnist.html (Accessed on 1-October-2020).

[23] B. Uria, M.-A. Côté, K. Gregor, I. Murray, and H. Larochelle, Neural autoregressive distribution estimation, *The Journal of Machine Learning Research* **17**, 7184 (2016).

[24] M. Germain, K. Gregor, I. Murray, and H. Larochelle, Made: Masked autoencoder for distribution estimation, in *International Conference on Machine Learning* (2015) pp. 881–889.

[25] A. Van den Oord, N. Kalchbrenner, L. Espeholt, O. Vinyals, A. Graves, *et al.*, Conditional image generation with pixelcnn decoders, in *Advances in neural information processing systems* (2016) pp. 4790–4798.

[26] R. Salakhutdinov and I. Murray, On the quantitative analysis of deep belief networks, in *Proceedings of the 25th international conference on Machine learning* (2008) pp. 872–879.

[27] R. S. Sutton and A. G. Barto, *Reinforcement learning: An introduction* (MIT press, 2018).

[28] D. Silver, J. Schrittwieser, K. Simonyan, I. Antonoglou, A. Huang, A. Guez, T. Hubert, L. Baker, M. Lai, A. Bolton, *et al.*, Mastering the game of go without human knowledge, *nature* **550**, 354 (2017).

[29] F. Pan, P. Zhou, H.-J. Zhou, and P. Zhang, Solving statistical mechanics on sparse graphs with feedback-set variational autoregressive networks, *Phys. Rev. E* **103**, 012103 (2021).

[30] G. Carleo and M. Troyer, Solving the quantum many-body problem with artificial neural networks, *Science* **355**, 602 (2017).

[31] O. Sharir, Y. Levine, N. Wies, G. Carleo, and A. Shashua, Deep autoregressive models for the efficient variational simulation of many-body quantum systems, *Physical Review Letters* **124**, 020503 (2020).

[32] J. R. Anderson and C. Peterson, A mean field theory learning algorithm for neural networks, *Complex Systems* **1**, 995 (1987).

[33] D. Sherrington and S. Kirkpatrick, Solvable model of a spin-glass, *Physical Review Letters* **35**, 1792 (1975).

[34] S. Boixo, S. V. Isakov, V. N. Smelyanskiy, R. Babbush, N. Ding, Z. Jiang, M. J. Bremner, J. M. Martinis, and H. Neven, Characterizing quantum supremacy in near-term devices, *Nature Physics* **14**, 595 (2018).

[35] F. Pan, P. Zhou, S. Li, and P. Zhang, Contracting arbitrary tensor networks: general approximate algorithm and applications in graphical models and quantum circuit simulations, *Physical Review Letters* **125**, 060503 (2020).

[36] F. Pan and P. Zhang, Simulating the sycamore quantum supremacy circuits, *arXiv preprint arXiv:2103.03074* (2021).

[37] <https://github.com/bnuluijing/tn-for-unsup-ml>.

[38] A. Cichocki, N. Lee, I. Oseledets, A.-H. Phan, Q. Zhao, and D. P. Mandic, Tensor networks for dimensionality reduction and large-scale optimization: Part 1 low-rank tensor decompositions, *Foundations and Trends® in Machine Learning* **9**, 249 (2016).

[39] I. V. Oseledets, Tensor-train decomposition, *SIAM Journal on Scientific Computing* **33**, 2295 (2011).

[40] I. Glasser, N. Pancotti, M. August, I. D. Rodriguez, and J. I. Cirac, Neural-network quantum states, string-bond states, and chiral topological states, *Physical Review X* **8**, 011006 (2018).

[41] H. Larochelle and I. Murray, The neural autoregressive distribution estimator, in *Proceedings of the Fourteenth International Conference on Artificial Intelligence and Statistics* (JMLR Workshop and Conference Proceedings, 2011) pp. 29–37.

[42] D. P. Kingma and J. Ba, Adam: A method for stochastic optimization, in *3rd International Conference on Learning Representations, ICLR 2015, San Diego, CA, USA, May 7-9, 2015, Conference Track Proceedings*, edited by Y. Bengio and Y. LeCun (2015).

[43] N. S. Müller, M. Studer, and G. Ritschard, Classification de parcours de vie à l'aide de l'optimal matching, *XIVe Rencontre*

de la Société francophone de classification (SFC 2007) , 157 (2007).

[44] D. Dua and C. Graff, [UCI machine learning repository](#) (2017).

[45] https://github.com/givan/tensor_networks_for_probabilistic_modeling (Accessed on 1-October-2020).

Two-dimensional tensor network representation of RBM

For the completeness, here we give a compact descriptions on how to construct the two-dimensional tensor network representation of the RBM as proposed in [13]. In the RBM, the joint distribution of n visible variables and m hidden variables are defined as

$$p(\mathbf{x}) = \frac{1}{Z} \sum_{\mathbf{h}} e^{J_{ij} x_i h_j + \theta_i x_i + \theta_j h_j} = \frac{1}{Z} \prod_{i=1}^n e^{x_i \theta_i} \prod_{j=1}^m \Phi_{x_1, x_2, \dots, x_n}^{(j)},$$

where J_{ij} denotes couplings between visible variable i and hidden variable j ; θ_i and θ_j denote external field of visible node i and hidden node j respectively, and

$$\Phi_{x_1, x_2, \dots, x_n}^{(j)} = 2 \cosh \left(\sum_{i=1}^n J_{ij} x_i + \theta_j \right).$$

That is, the joint distribution is factorized to the product of Φ functions, each of which accepts a configuration of visible variable \mathbf{x} as input, and outputs a scalar value. When the visible variables are discrete, each Φ can be treated as a tensor \mathcal{A}_j in the linear space with dimension 2^n . Furthermore, \mathcal{A}_j is a sum over two rank-one tensors $\prod_{i=1}^n e^{J_{ij} x_i + \theta_j}$ and $\prod_{i=1}^n e^{-J_{ij} x_i - \theta_j}$, hence is in a Canonical Polyadic (CP) form [38] with CP rank equals 2. It is well known that a CP tensor can be converted exact to a matrix product state with bond dimension equals its CP rank [39]. In this sense, an RBM can be regarded as a Correlator Product States [16, 40]. Further, we notice that each visible variable i can be regarded as a copy tensor with dimension $m+1$. A copy tensor can be also converted to a MPS \mathcal{B}_i with bond dimension 2. Connecting every pair of \mathcal{B}_i and \mathcal{A}_j by contracting the associated couplings matrices between them, we arrive at a two-dimension tensor network representation of RBM as illustrated in Fig. 1(c), where each row corresponds to an MPS with \mathcal{A} , and each column corresponds to an MPS with \mathcal{B} , all have bond dimension equals 2. For more details about the two-dimensional representation we refer to [13].

Detailed description of the Autoregressive Matrix Product States

Here we give a more detailed description of the Autoregressive Matrix Product States (AMPS). To fully exploit the representation power with the product of MPSs, we decompose the joint probability using the chain rule of probabilities, which has recently been used e.g. in Variational Autoregressive Networks (VAN) [14]. As a concrete example, let us consider a model with four binary variables $\{x_1, x_2, x_3, x_4\}$, the joint distribution is written as

$$\begin{aligned} P(x_1, x_2, x_3, x_4) &= P(x_1)P(x_2|x_1)P(x_3|x_1, x_2)P(x_4|x_1, x_2, x_3) \\ &= \Psi_{x_1}^{(1)} \Psi_{x_1, x_2}^{(2)} \Psi_{x_1, x_2, x_3}^{(3)} \Psi_{x_1, x_2, x_3, x_4}^{(4)} \end{aligned} \quad (5)$$

In particular, $\Psi_{x_1, x_2, x_3, x_4}^{(4)}$ expresses the conditional probability $P(x_4|x_1, x_2, x_3)$. In order to express such a normalized conditional probability, we first construct an MPS

$$\Psi_{x_1, x_2, x_3, x_4} = \sum_{\{\alpha_0, \alpha_1, \alpha_2, \alpha_3, \alpha_4\}} A_{x_1 \alpha_0 \alpha_1}^{(1)} A_{x_2 \alpha_1 \alpha_2}^{(2)} A_{x_3 \alpha_2 \alpha_3}^{(3)} A_{x_4 \alpha_3 \alpha_4}^{(4)}, \quad (6)$$

where $A^{(i)} \in \mathbb{R}^{2 \times D_{i-1} \times D_i}$ is a three-way tensor and $D_0 = D_4 = 1$. Next the conditional probability $P(x_4|x_1, x_2, x_3)$ is given by the exponential of $\Psi_{x_1, x_2, x_3, x_4}$

$$\Psi_{x_1, x_2, x_3, x_4}^{(4)} = \frac{\exp(\Psi_{x_1, x_2, x_3, x_4})}{\sum_{x_4} \exp(\Psi_{x_1, x_2, x_3, x_4})}. \quad (7)$$

Notice that this is not the only way to define such a conditional probability. It can also be constructed by the squared norm in MPS Born machine [7] as

$$\Psi_{x_1, x_2, x_3, x_4}^{(4)} = \frac{|\Psi_{x_1, x_2, x_3, x_4}|^2}{\sum_{x_4} |\Psi_{x_1, x_2, x_3, x_4}|^2}, \quad (8)$$

or by introducing non-negative three-way tensors such that $\psi_{x_1, x_2, x_3, x_4} \geq 0$, and express the conditional probability as

$$\Psi_{x_1, x_2, x_3, x_4}^{(4)} = \frac{\psi_{x_1, x_2, x_3, x_4}}{\sum_{x_4} \psi_{x_1, x_2, x_3, x_4}}. \quad (9)$$

In practice, the exponential way works best in our numerical experiments. Since each conditional probability $P(x_i|x_1, \dots, x_{i-1})$ is parameterized by a MPS of length i , the number of parameters for AMPS model scales $n^2 D^2$.

In order to reduce the number of parameters needed to describe the joint distribution, we introduce a parameter sharing scheme, which is widely used in state-of-the-art neural network architecture such as Convolutional Neural Networks (CNN). A simple parameter sharing scheme for AMPS model is to force all MPSs sharing the whole parameters. For example, the conditional probability $P(x_3|x_1, x_2)$ is constructed by the MPS

$$\psi_{x_1, x_2, x_3} = \sum_{\{\alpha_0, \alpha_1, \alpha_2, \alpha_3\}} A_{x_1 \alpha_0 \alpha_1}^{(1)} A_{x_2 \alpha_1 \alpha_2}^{(2)} \tilde{A}_{x_3 \alpha_2 \alpha_3}^{(3)} \quad (10)$$

where $A_{x_1 \alpha_0 \alpha_1}^{(1)}$ and $A_{x_2 \alpha_1 \alpha_2}^{(2)}$ are the same tensors used in Eq. (6). The last tensor $\tilde{A}_{x_3 \alpha_2 \alpha_3}^{(3)} = A_{x_3 \alpha_2 \alpha_3}^{(3)}[:0]$ is the first frontal slice of $A_{x_3 \alpha_2 \alpha_3}^{(3)}$ in Eq. (6), which is a $2 \times D_2 \times 1$ tensor. We call this model *Shared-AMPS*. Notice that this parameter sharing scheme is very similar to that used in Neural Autoregressive Distribution Estimator (NADE) [41].

In practice, we find that this parameter sharing scheme is useful to improve the model generalization ability and greatly reduces the number of parameters. For *Shared-AMPS*, since every conditional probability is parameterized by the same set of three-way tensors, the number of parameters only scales nD^2 .

For two-dimensional structure such as natural images, the PixelCNN [25] model is proposed to generate the images pixel by pixel using masked convolutional layers. In order to take advantage of convolutions in modeling images, we introduce a convolutional structure based on AMPS, which is called *Convolution-AMPS*. The main difference in of the convolution-AMPS to AMPS is that the scope of each MPS (for representing conditional probability) is restricted to neighbors of a pixel with a certain distance, and many MPSs are used to represent the conditional probability, acting like different convolution kernels in convolutional neural networks. In the first layer, the MPS kernel will act on the input data and produce a vector for each pixel, which is regarded as the input of the next layer. Until the last layer, a normalized conditional probability for each pixel is given by the exponential in Eq. (7).

More results and training details on random datasets

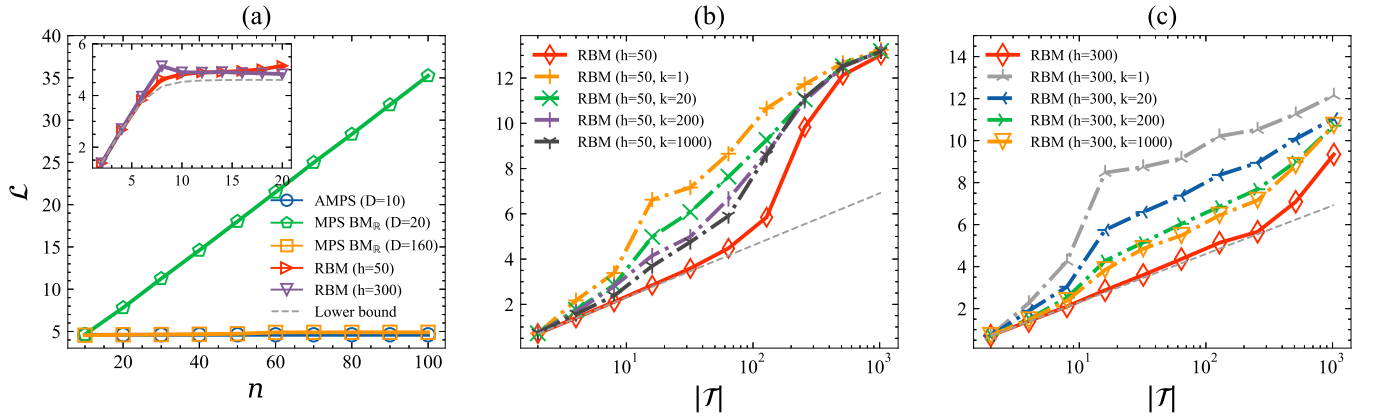


Figure 5. (a) For random dataset with fixed sample size $|\mathcal{T}| = 100$, we show the NLL \mathcal{L} of various models in different system size n . (b) (c) For random dataset with $n = 20$, the performance of RBM with hidden variables $h = 50$ and $h = 300$.

We first give a gentle introduction to the task of generative modeling. In generative modeling, we try to train a model to represent the target data distribution. Given empirical data distribution $P_{\text{data}}(\mathbf{x})$ and model distribution $P(\mathbf{x}; \boldsymbol{\theta})$ parameterized

by θ , the Kullback-Leibler (KL) divergence measures the closeness of two probability distribution:

$$\begin{aligned} D_{\text{KL}}(P_{\text{data}}(\mathbf{x}) \parallel P(\mathbf{x}; \theta)) &= \sum_{\mathbf{x}} P_{\text{data}}(\mathbf{x}) \ln \left(\frac{P_{\text{data}}(\mathbf{x})}{P(\mathbf{x}; \theta)} \right) \\ &= \sum_{\mathbf{x}} P_{\text{data}}(\mathbf{x}) \ln P_{\text{data}}(\mathbf{x}) - \sum_{\mathbf{x}} P_{\text{data}}(\mathbf{x}) \ln P(\mathbf{x}; \theta). \end{aligned} \quad (11)$$

The first term on the RHS is the entropy of the empirical data distribution, which is equal to $-\ln |\mathcal{T}|$ if there are no duplication in the dataset. By replacing $P_{\text{data}}(\mathbf{x})$ with $\frac{1}{|\mathcal{T}|} \sum_{\mathbf{x}' \in \mathcal{T}} \delta(\mathbf{x} - \mathbf{x}')$, the second term is the negative log-likelihood (NLL):

$$\begin{aligned} \mathcal{L} &= - \sum_{\mathbf{x}} P_{\text{data}}(\mathbf{x}) \ln P(\mathbf{x}; \theta) \\ &= -\frac{1}{|\mathcal{T}|} \sum_{\mathbf{x} \in \mathcal{T}} \ln P(\mathbf{x}; \theta). \end{aligned} \quad (12)$$

Since the KL divergence is non-negative, we have $\mathcal{L} \geq -\sum_{\mathbf{x}} P_{\text{data}}(\mathbf{x}) \ln P_{\text{data}}(\mathbf{x})$, which means that the entropy of the empirical data distribution provides the lower bound for the NLL. When $\mathcal{L} = -\sum_{\mathbf{x}} P_{\text{data}}(\mathbf{x}) \ln P_{\text{data}}(\mathbf{x})$, the model distribution is exactly the empirical data distribution. The pseudocode for generative modeling is presented in the Algorithm (1).

Algorithm 1 AMPS for generative modeling

Input: MPS parameters θ , dataset $\mathcal{T} = \{\mathbf{x}_1, \mathbf{x}_2, \dots, \mathbf{x}_{|\mathcal{T}|}\}$, batch size N_{bs} , learning rate η
Output: Well trained model $P(\mathbf{x}; \theta)$, NLL \mathcal{L} .

```

Initialize MPS parameters  $\theta$ 
while Stopping criterion is not satisfied do
    Sample a batch of  $N_{\text{bs}}$  data points from dataset  $\mathcal{T}$ .
    Compute NLL  $\mathcal{L}_\theta$  using Eq. (12)
    Compute the gradients  $\nabla_\theta \mathcal{L}_\theta$ 
    Update MPS parameters using the gradients and an optimizer (such as Adam [42]).
end while
if Sample from the learned distribution then
    for  $i = 1, 2, \dots, n$  do
        Compute  $P(x_i | x_1, \dots, x_{i-1})$ 
        Sample  $x_i$  from  $P(x_i | x_1, \dots, x_{i-1})$ 
    end for
end if
Return NLL  $\mathcal{L}$  and new samples from the learned distribution.

```

For random samples drawn from Bernoulli distribution, since we are only interested in the expressive power, we try to obtain an NLL that as small as possible. In all the experiments, we have used batch size equal to the number of samples $|\mathcal{T}|$, learning rate 0.001 and 10,000 training steps to ensure that the optimization converges. In addition to the experiments with a fixed number of variables presented in the main text, we also conducted numerical experiments with a fixed number of samples $|\mathcal{T}| = 100$, the performance is shown in Figure 5(a). Notice that for a small value of n , the total number of configurations 2^n is smaller than $|\mathcal{T}| = 100$, so the lower bound for \mathcal{L} should be calculated according to $-\sum_{\mathbf{x}} P_{\text{data}}(\mathbf{x}) \ln P_{\text{data}}(\mathbf{x})$. We can see from the figure that with a larger bond dimension D , the MPS Born machine obtains smaller \mathcal{L} . When bond dimension $D = 160$ which is larger than $|\mathcal{T}|$, the MPS Born machine gives $\mathcal{L} = \ln |\mathcal{T}|$. Remarkably, our AMPS model can achieve the same performance with a much smaller bond dimension $D = 10$.

In the training process of RBM, the gradients can be exactly computed involving exhaustive enumerating of all configurations, or approximately calculated such as Contrastive Divergence (CD) algorithm. Figure 5(b) and (c) display the NLL on the training dataset obtained with different gradient-computing methods with hidden variables $h = 50$ and 300. Apparently, when the number of steps in Gibbs sampling increases, the model performs better and gives a closer to the exact gradients. However, none of these RBM models can reach the theoretical lower bound $\ln |\mathcal{T}|$.

More results and training details for real-world datasets

To fully demonstrate the expressive power, we have also performed extensive experiments on various real-world datasets studied in [10]: Biofam dataset from the Swiss Household Panel biographical survey [43], datasets from the UCI Machine

Learning Repository [44]: Lymphography [20], SPECT Heart, Congressional Voting Records, Primary Tumor [20] and Solar Flare. The dataset statistics are summarized in Table II.

Table II. Statistics of real-world datasets. Here $|\mathcal{T}|$ denotes the total number of samples, n denotes the number of variables and d denotes the number of categories.

Dataset	$ \mathcal{T} $	n	d
Biofam	2000	16	8
Lymphography	148	19	8
SPECT Heart	187	23	2
Congressional Voting Records	435	17	3
Primary Tumor	339	17	4
Solar Flare	1065	13	8

We compare against the following tensor-network methods:

- Positive MPS ($\text{MPS}_{\mathbb{R} \geq 0}$): decomposing the joint distribution $P(\mathbf{x})$ into an MPS with non-negative tensors.
- MPS Born machines ($\text{MPS BM}_{\mathbb{R}}$): the $P(\mathbf{x})$ is modeled by squared norm of a quantum state Ψ , with $P(\mathbf{x}) = \frac{1}{Z} |\Psi(x_1, x_2, \dots, x_n)|^2$.
- MPS Born machines with complex entries ($\text{MPS BM}_{\mathbb{C}}$): same as MPS Born Machines but with complex tensors.
- Locally Purified States ($\text{LPS}_{\mathbb{R}}$): proposed in [10], introducing additional purification dimension in MPS tensors.
- Locally Purified State with complex entries ($\text{LPS}_{\mathbb{C}}$): same as Locally Purified States but with complex tensors.

In all experiments, we have used a batch size equal to the number of samples $|\mathcal{T}|$. For different models, the number of parameters as well as learning rate and training steps are summarized in Table III. The implementations of the the reference tensor-network methods as well as the datasets were downloaded from [45].

Table III. Summary of number of parameters, learning rate and training steps for different models.

Model	# parameters	learning rate	training steps
AMPS	$dn(n+1)D^2/2$	0.001	10,000
Shared AMPS	dnd^2	0.001	10,000
$\text{MPS}_{\mathbb{R} \geq 0}$	dnd^2	1	10,000
$\text{MPS BM}_{\mathbb{R}}$	dnd^2	1	10,000
$\text{MPS BM}_{\mathbb{C}}$	$2dnd^2$	1	10,000
$\text{LPS}_{\mathbb{R}}$	$2dnd^2$	10	10,000
$\text{LPS}_{\mathbb{C}}$	$4dnd^2$	10	10,000

We plot the NLL \mathcal{L} as a function of bond dimension D for different models in Figure 6. We can observe from the figure that the AMPS model significant outperforms other tensor network models by a large gap. Remarkably, even *Shared-AMPS* with very few parameters is already significantly superior with the same bond dimension.

In Figure 7 we investigate how the number of parameters influence the performances. We can see from the figure that for a given number of parameters, the AMPS model can achieve much lower NLL compared to other models, indicating that AMPS model has much stronger expressive power than the existing tensor-network-based models.

More results and training details for binarized MNIST dataset

In the above experiments on random and real-world datasets, we only cared about expressive power of the model while completely ignored the generalization, i.e., evaluating the NLL on the test dataset and the ability of generating new samples. Here we investigate the generalization power of Shared-AMPS and Convolution-AMPS on the binarized MNIST dataset, a standard dataset in machine learning. After training the models on the MNIST dataset, we can sample from the learned distribution through the ascenstral sampling [1, 7]. As a concrete example, consider again the case with four binary variables. To samples a new data point \mathbf{x} , we first determine x_1 from $\Psi_{x_1}^{(1)}$, then determine x_2 from $\Psi_{x_1, x_2}^{(2)}$ using x_1 , then determine x_3 from $\Psi_{x_1, x_2, x_3}^{(3)}$ using x_1 and x_2 , finally determine x_4 from $\Psi_{x_1, x_2, x_3, x_4}^{(4)}$ using x_1, x_2 and x_3 .

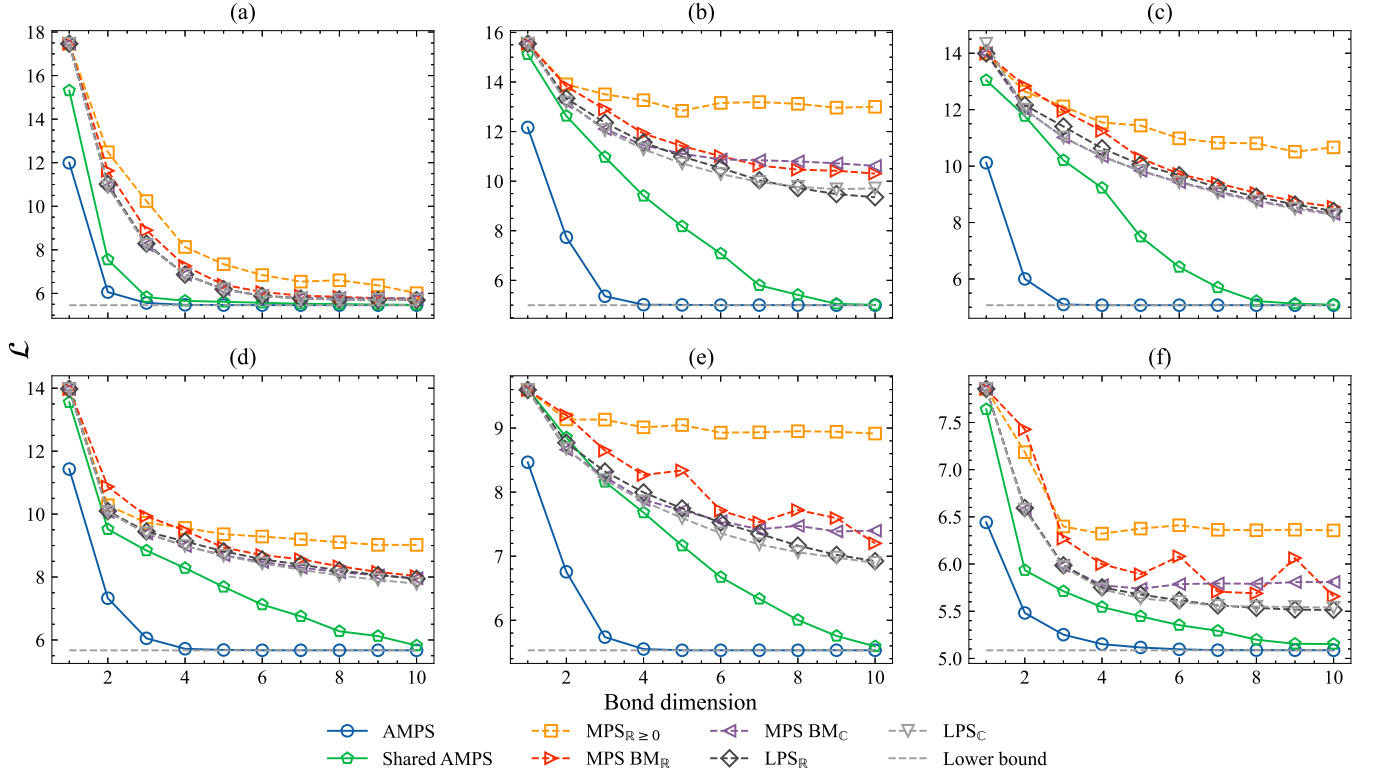


Figure 6. NLL as a function of bond dimension for different models on the real-world datasets: (a) Biofam [43], datasets from the UCI Machine Learning Repository [44]; (b) Lymphography [20], (c) SPECT Heart, (d) Congressional Voting Records, (e) Primary Tumor [20], (f) Solar Flare.

For *Shared-AMPS*, we have used batch size 100, initial learning rate 0.1, epochs 50 and decaying the learning rate by 0.1 every 10 epochs. As for *Convolutional-AMPS*, we construct an eight-layer convolutional network with the bond dimension of MPS equal to 14 and the convolution kernel size is 7×7 . We used batch size 200, initial learning rate 10^{-4} and weight decay 10^{-4} . The NLL on the test dataset as well as the samples drawn from the learned distribution are shown in the main text. In addition, in Figure (8) we plot the training NLL and test NLL as a function of bond dimension for *Shared-AMPS* model. We find that as the bond dimension increases, the performance on the test dataset no longer improves, indicating an overfitting phenomenon with more parameters than we need on the dataset. The best test NLL is 84.1 with the dimension is $D = 100$, as reported in the main text. To the best of our knowledge, this is the best result given by tensor-network-based methods.

More results and training details for SK model

In reinforcement learning for statistical physics, we try to make the variational distribution $q(\mathbf{x}; \boldsymbol{\theta})$ as close as possible to the equilibrium Boltzmann distribution $P(\mathbf{x}) = \exp(-\beta E(\mathbf{x}))/Z$. The closeness of two probability distribution is measured by the reverse KL divergence:

$$D_{\text{KL}}(q(\mathbf{x}; \boldsymbol{\theta}) \parallel P(\mathbf{x})) = \sum_{\mathbf{x}} q(\mathbf{x}; \boldsymbol{\theta}) \ln \left(\frac{q(\mathbf{x}; \boldsymbol{\theta})}{P(\mathbf{x})} \right) = \beta(F_q - F), \quad (13)$$

where

$$F_q = \frac{1}{\beta} \sum_{\mathbf{x}} q(\mathbf{x}; \boldsymbol{\theta}) [\beta E(\mathbf{x}) + \ln q(\mathbf{x}; \boldsymbol{\theta})] \quad (14)$$

is the variational free energy and F is the true free energy. In our numerical experiments, the variational distribution is parameterized by our AMPS model. For the Sherrington-Kirkpatrick (SK) model [33], the energy $E(\mathbf{x})$ is defined as

$$E(\mathbf{x}) = - \sum_{1 \leq i < j \leq n} J_{ij} s_i s_j. \quad (15)$$

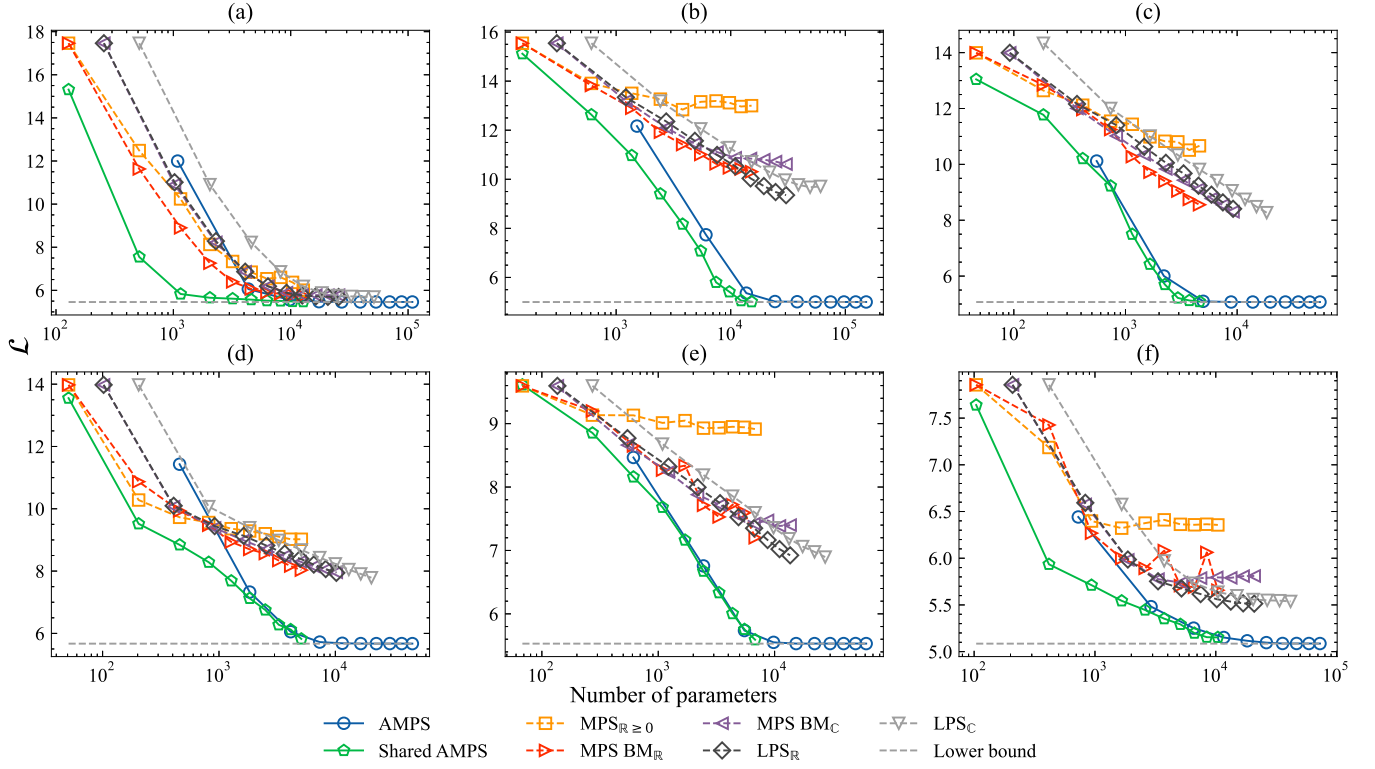


Figure 7. NLL as a function of number of parameters for different models on the real-world datasets: (a) Biofam data set: The family life states data from the Swiss Household Panel biographical survey [43] and the datasets come from the UCI Machine Learning Repository [44]: (b) Lymphography and tumor domains [20], (c) SPECT Heart, (d) Congressional Voting Records, (e) Primary Tumor [20], (f) Solar Flare. The lower bounds for \mathcal{L} are determined using entropy of the empirical data distribution. All datasets are downloaded from from [45].

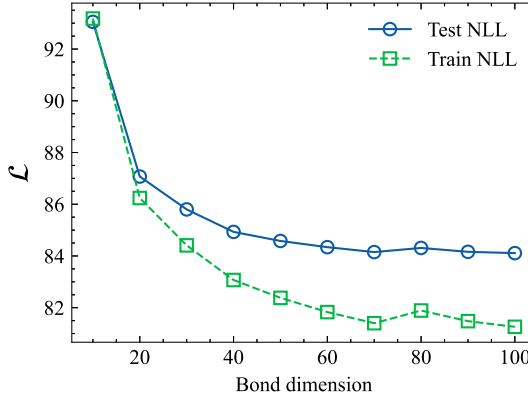


Figure 8. Training NLL and test NLL as a function of the bond dimension D in the Shared-AMPS trained on the binary MNIST dataset using all 50,000 training images.

By denoting $\hat{x}_i = P(s_i = +1)$, the entropy is given by

$$\ln q(\mathbf{x}; \boldsymbol{\theta}) = \sum_{i=1}^n [x_i \ln \hat{x}_i + (1 - x_i) \ln (1 - \hat{x}_i)]. \quad (16)$$

We adopt the score function estimator [15] for estimating the gradient of the variational free energy with respect to model parameters and for optimizing the variational free energy F_q :

$$\nabla_{\boldsymbol{\theta}} F_q = \frac{1}{\beta} \sum_{\mathbf{x}} q(\mathbf{x}; \boldsymbol{\theta}) [\beta E(\mathbf{x}) + \ln q(\mathbf{x}; \boldsymbol{\theta})] \nabla_{\boldsymbol{\theta}} \ln q(\mathbf{x}; \boldsymbol{\theta}). \quad (17)$$

The pseudocode for reinforcement learning for statistical physics is presented in the Algorithm (2).

Algorithm 2 AMPS for reinforcement learning in statistical physics

Input: MPS parameters θ , coupling $\{J_{ij}\}$, batch size N_{bs} , learning rate η
Output: Trained variational distribution $q(\mathbf{x}; \theta)$, variational free energy F_q .

```

Initialize MPS parameters  $\theta$ 
while Stopping criterion is not satisfied do
    Generate a batch of  $N_{\text{bs}}$  samples from the variational distribution  $q(\mathbf{x}; \theta)$  by the ascenstral sampling
    Compute the energy and the entropy using Eq.(15) and Eq.(16), then compute variational free energy  $F_q$  using Eq.(14).
    Compute the gradients  $\nabla_{\theta} F_q$  using the score function estimator Eq.(17)
    Update MPS parameters using the gradients and an optimizer e.g. Adam [42].
end while
Return Variational free energy  $F_q$ .
```

In our experiments, we follow the same experimental setup in [14]. We have used batch size 10,000 and learning rate 0.001. The main results are shown in the main text. We also found that when the number of parameters of VAN and AMPS is close, their performance is also very close to each other. In Table (IV) we show the model details and the corresponding number of parameters. In Figure (9) we plot the relative error of free energy respectively.

Table IV. Model details for SK model with system size $N = 20$.

Model	Detail	# Parameters
AMPS	D=2	1600
	D=4	6400
	D=6	14400
	D=8	25600
	D=10	40000
2 layer VAN	20 hidden neurons	800
	100 hidden neurons	4000
	200 hidden neurons	8000
3 layer VAN	20 hidden neurons	1200
	100 hidden neurons	14000
	200 hidden neurons	48000

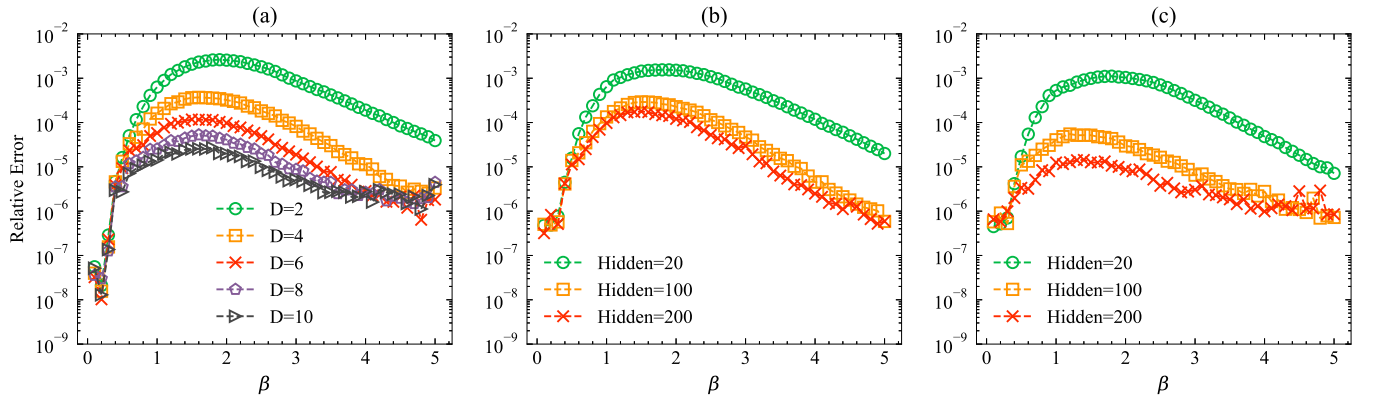


Figure 9. Relative error of free energy for (a) AMPS with different bond dimension, (b) a 2 layer VAN with different hidden neurons and (c) a 3 layer VAN with different hidden neurons.